Light Metals 2014
Edited by: John Grandfield
TMS (The Minerals, Metals & Materials Society), 2014

MHD STABILITY FOR IRREGULAR AND DISTURBED ALUMINIUM REDUCTION CELLS

Valdis Bojarevics and Sharnjit Sira
University of Greenwich, Park Row, London, SE10 9LS, UK

Keywords: aluminium reduction cells, magnetohydrodynamics, wave instability

Abstract

The MHD stability of regular cells in pot line is well represented in the literature, and validated numerical tools are available to optimize their performance. The presence of irregular cells is more of a rule than an accident in the commercial practice requiring additional flexibility when modeling such cells interspersed between normal ones. The new options in the code for MHD analysis permit to include such technological variations as change of anodes at arbitrary position, parallel change of several anodes, variation of the contact resistances in anode clamps, cathode flex joints, collectors, electrolyte and overvoltage. The extended model capabilities include the presence of anode channels, cell bottom non-uniformities and variable bottom ledge. Options to build a user specified magnetically compensating bus network, to account for a stopped neighbor pot (shunted) and end of line pots with significantly disturbed magnetic field are numerically tested for the 500 kA cell pot line.

1. Introduction

Industrial aluminium production cells are highly optimized for magnetic field and electric current distribution in order to avoid MHD instabilities, increase the current efficiency and to maintain a stable electrolytic process during normal operation. The ability to predict the cell magnetic and electric field distribution to high accuracy is a key to control disturbances and deviations from a normal production process. In normal plant operation various disturbances appear, such as repair of the neighbor cells, tapping liquid metal, anode change (single or a number of anodes at the same time), end of line cell particular adjustments, and so on, in various combinations and unpredictable day to day routines. Use of mathematical modeling to alleviate risks and choose optimum possible solution is a new and untested challenge. The MHD software for the magneto-hydrodynamic (MHD) features of the cells and the prediction of unstable behavior has reached certain maturity since the first principles of the MHD were introduced [1]. The universal MHD code [2] using physically reasonable approximation of the 3dimensional electromagnetic fields and the extended shallow layer turbulent fluid flow model permits to simulate real commercial cells accounting for a variety of their individual features. The code is extensively tested [3,4 and other unpublished cases]. It is also fully verified against the benchmark case [2,5].

The MHD interaction is the global field effect realized when an integrated model of the pot-line aluminium cell arrangement is properly accounted. Most of the cells are in the mid position between their neighbors, however the model permits to prescribe the cell location for increased versatility. Options to build a user specified magnetically compensating bus network, to account for a stopped neighbor pot (shunted) and end of line pots with significantly disturbed magnetic field are numerically tested. The new options in the code for MHD analysis permit to include such technological variations as change of anodes at arbitrary position, parallel change of several anodes, variation of the contact resistances in anode clamps, cathode flex joints, collectors, electrolyte overvoltage. The extended model capabilities include the presence of anode channels, cell bottom non-uniformities and variable bottom ledge.

2. Some aspects of mathematical model

The electric current in the liquid metal has large horizontal component due to the high electrical conductivity of metal and the exit path to the cell side where the bottom ledge starts. The shape of the cathode in the form of protrusions or depressions could affect the horizontal current density and redistribution. These three dimensional features of the electric current flow can be efficiently modeled using the small depth to horizontal dimension ratio expansion model [6]. In general equations governing the DC current for the electric potential are:

$$\mathbf{j} = -\sigma \nabla \varphi, \tag{1}$$

$$\nabla^2 \varphi = 0 \tag{2}$$

The boundary conditions are the zero normal current at the insulating walls, the given total current entering the anode rod and the fixed reference potential at the exit cathode collector end. At the interfaces between the liquid metal, electrolyte, carbon and all other materials the continuity of the potential and the normal component of electric current must be satisfied.

The magnetic field in the aluminium electrolysis cell is created by the currents in the cell itself, from the complex bus-bar arrangement around the cell, from the currents of the neighboring cells and the return line, and by the magnetization effect of the cell construction steel. The full 3d busbar configuration extended with the neighbor cells and the ferromagnetic parts of the cell is used for the model simulations. The magnetic field $\mathbf{B_I}$ from the currents in the full bus-bar network is calculated using the Biot-Savart law

$$\mathbf{B}_\mathbf{I} = \frac{\mu_0}{4\pi} \int \frac{\mathbf{j} \times \mathbf{R}}{R^3} dV \tag{3}$$

The equation (3) is used on the 3D grid within the cell fluid layers where a special analytical technique is applied to deal with the singularity in the Biot-Savart law in order to obtain solution when the field calculation position is located in the vicinity of the electric current location [6]. For the external busbar circuit, consisting of tens of thousands of current elements, the integral (3) is approximated either by line elements for distant currents, by numerical volume integral, or by analytical expressions [6] implemented in this code for an efficient numerical usage. The selective choice of the field approximation is essential to avoid the effect of singularity in the Biot-Savart law in order to obtain a smooth, convergent solution when the field calculation position is located in the vicinity to the electric current, the so-called self-magnetic field effect.

Another aspect of the numerical code, which is particularly important to model individuality of the cells in line, is the variable bottom effect on the turbulent friction. The effective viscosity is defined as the sum of laminar and turbulent viscosity,

$$\nu_e(x,y,t) = \nu + \nu_T(k,\omega), \tag{4}$$

it is obtained by solving the time dependent k-ω two-equation model [7,8]. The k-ω model is a variant of low Reynolds number turbulence models which permits to resolve the flow from laminar to the fully developed turbulent state. The ω variable is related to the reciprocal turbulent time scale (frequency of vorticity fluctuations) and the k variable is the turbulence kinetic energy. The k-ω model governing equations are:

$$\partial_t k + \mathbf{v}\cdot\nabla k = \nabla\cdot[(\nu+\sigma_k\nu_T)\nabla k] + G - \beta^*\omega\, k + C_f\,|\mathbf{v}|^3\, H_i^{-1} \tag{5}$$

$$\partial_t \omega + \mathbf{v}\cdot\nabla \omega = \nabla\cdot[(\nu+\sigma_\omega\nu_T)\nabla \omega] + \alpha\frac{\omega}{k}G - \beta\,\omega^2 + 2C_f\,|\mathbf{v}|^4\, H_i^{-2}\frac{1}{\beta^* k},$$

where the turbulent viscosity is ν_T, the turbulent kinetic energy generating term G is defined by the mean velocity strain rate, and the large number of different model constants and 'wall damping' functions can be found in [7]. The depth averaging in the shallow layer approximation over the variable depths H_i of the electrolyte and liquid metal add new terms in the equations (5), permitting to account for the variable height bottom damping [8], i.e., the protrusion effect.

2. Comparison to simple 2d test for the electric current model

The numerical MHD model for the dynamic modeling uses the very efficient approximation based on the shallow nature of the fluid layers contained in the cell. However, certain aspects of the current distribution need to be verified by direct computation on a fine mesh using the approximation of a two-dimensional cross-section of the cell. The test model includes the resistive layers with the same material properties as in the full 3d model. The electric current is supplied to a single anode rod in the middle of the carbon anode, see the Figure 1 for the base case. The poor electrical contact void space at the end of the rod is included in the model. The electrolyte layer is 0.05 m and the liquid metal is 0.25 m thick. The side ledge is accounted for by a sloped electrically non-conducting wall. The carbon layer is initially set as flat, then several protrusions added as in the Figure 3. The important contribution to the current path is the contact resistance between the cathode carbon and the iron collector rod. The contact resistance is modeled as an additional thin uniformly distributed layer between the cathode carbon bottom surface and the iron bar top surface. The electrical resistivity of this contact resistance is adjusted to have the prescribed value of 0.0125 mOhm per single collector, according to typical industrial measurements. In the two dimensional case the cathode iron rod resistivity is effectively increased in proportion of the cathode block to the rod width ratio in order to account for the 3d to 2d transition in the 2d model. The model results are presented in the Figures 1-4 for the current flow in the liquid metal and cathode carbon. The line graphs in the Figures 5 and 6 compare quantitavely the currents for the 4 cases. It is evident that the contact resistance CR has significant influence to equalize the vertical current distribution (Figure 5), and to reduce significantly the depth average horizontal current density (Figure 6). The presence of the cathode protrusion elements, known to enhance the cell performance according to the recent publications [9-11], produce a significant local increase of the horizontal current, however the average horizontal current is less affected.

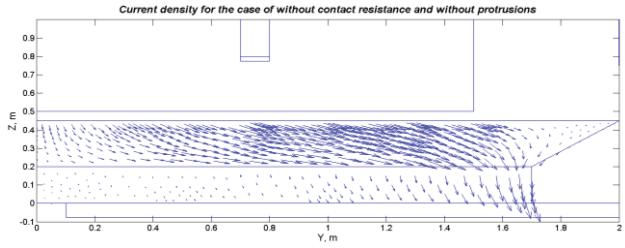

Figure 1. The 2d solution for the electric current in liquid metal and cathode carbon for the normal cell without the contact resistance.

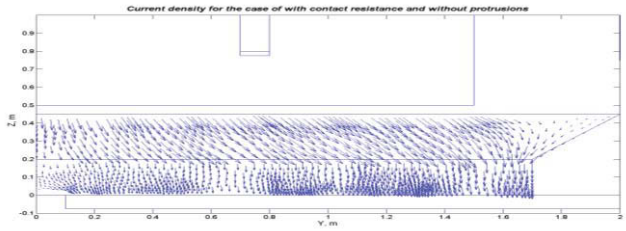

Figure 2. The 2d cross-section solution for the electric current when the contact resistance (carbon/iron rod) is included.

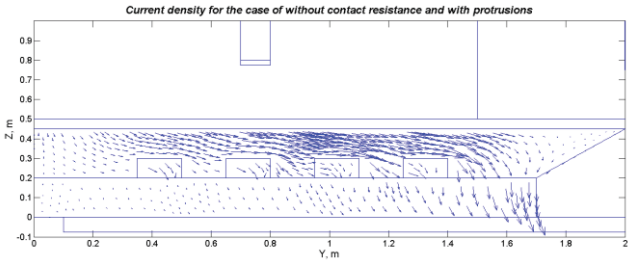

Figure 3. The 2d cross-section solution for the electriccurrent with the cathode perturbations included, no contact resistance.

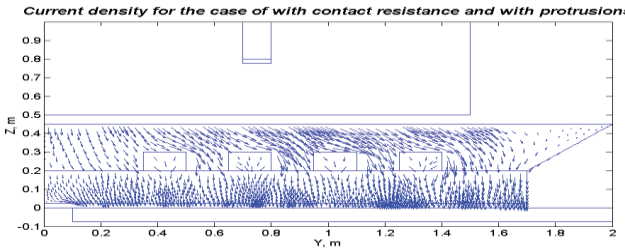

Figure 4. The 2d solution for the electric current when the cathode perturbations and the contact resistance are included.

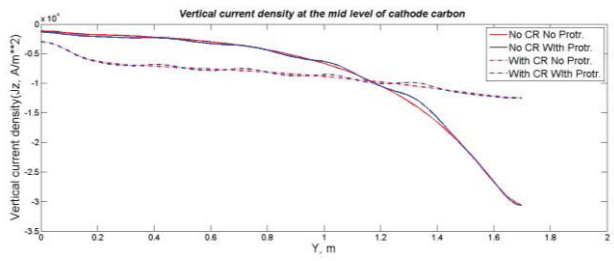

Figure 5. Comparison of the 2d solution for the vertical electric current entering the carbon cathode for the cases with/without the contact resistance (CR) and the cathode protrusions. (Half of the cell is shown, the origin is in the centre of the cell).

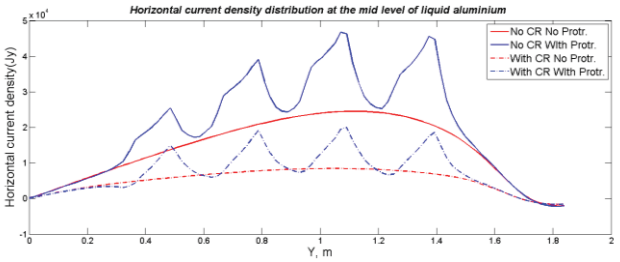

Figure 6. Comparison of the 2d solution horizontal electric current in liquid metal for the cases with/without the contact resistance (CR) and the cathode protrusions.

Table 1. Comparison of cathode type effect on the current and potential drop

Cathode types	Resistive potential drop (V)	Average horizontal current (in metal) (A/m^2)
Without contact resistance and without protrusions	2.5534	1.4897e+04
Without contact resistance and with protrusions	2.5554	1.8984e+04
With contact resistance and without protrusions	2.8204	5.4175e+03
With contact resistance and with protrusions	2.8217	6.9770e+03

The presence of the contact resistivity is felt more in the current distribution if compared to the protrusion effect (see the comparison in the Table 1).

These conclusions generally agree with our previous results demonstrating the effect of different ridge types at the cell bottom on the MHD stability [12]. The present 2d model ridges can be incorporated in the shallow layer cell model for further tests. Since the depths of the liquid layers are extremely small if compared to their horizontal extension, the shallow layer approximation is an accurate and efficient way to solve this 3-dimensional problem. The current distribution at the top and the bottom depend on the iterative solution from the linear element resolution of the bus bars, anodes, pins, collector bars, etc. in the full network. The bottom shape used for the full MHD model is shown in the Figure 7. The computed electric current in the liquid metal layer is shown in the Figure 8 for the flat bottom and in the Figure 9 for the perturbed carbon bottom.

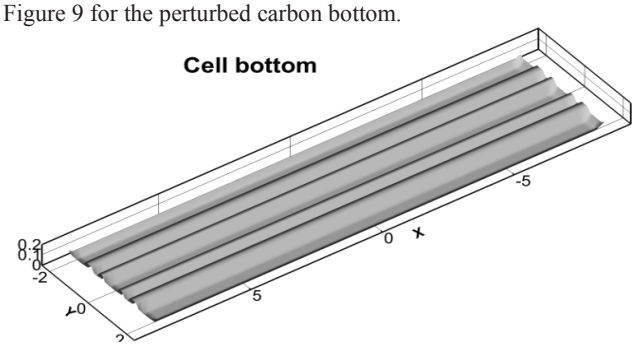

Figure 7. The cell bottom for the perturbed cathode used in the shallow layer model to compare the 2d ridge effects.

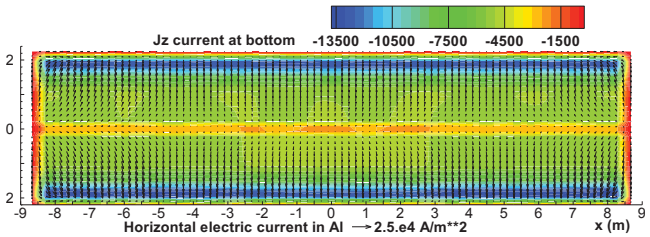

Figure 8. The shallow layer solution for the electric current in liquid metal and at the top of cathode carbon for the normal cell, including the 20 cm side ledge.

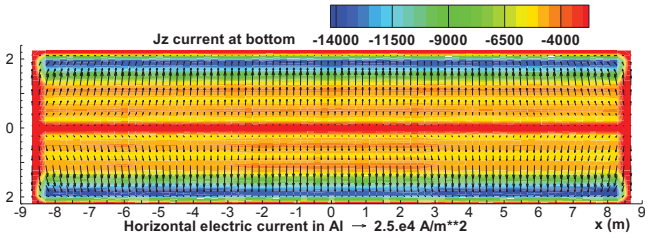

Figure 9. The shallow layer solution for the electric current for the perturbed cathode cell, including the 20 cm side ledge.

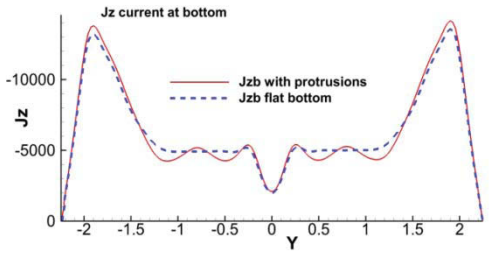

Figure 10. Vertical electric current distribution at the bottom of the cell for the perturbed cathode from the full MHD model.

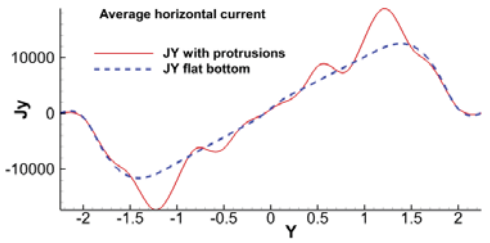

Figure 11. Horizontal current distribution in the middle of the cell for the perturbed cathode computed with the full MHD model.

The vertical current distribution (Figure 10) in this cell is very similar to the cathode wear profile reported and discussed in [13], hence suggesting certain implications to the older cell stability problems. The horizontal current reflects the presence of the cathode perturbations similarly to the 2d test case.

The 500 kA cell in this investigation is rather stable against the development of the MHD waves if the liquid metal volume is preserved to the volume of the metal in the cell without protrusions (15.57 m^3). If the level of the liquid metal (0.20m) is kept constant the volume is reduced in the presence of the protrusion elements (12.73 m^3), and the cell is unstable against the MHD waves as it is demonstrated in the Figure 12.

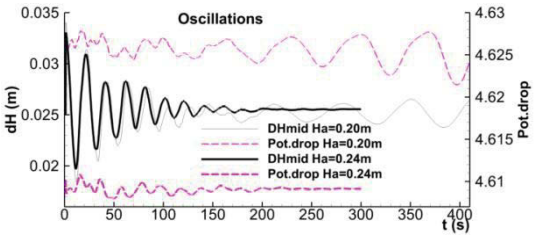

Figure 12. The interface perturbation and the total potential drop time evolution in the cell with the cathode perturbations.

It is instructive to have a view to the liquid metal deformed shape in these cells for the comparison of the cathode perturbation effect as shown in the Figures 13 and 14 respectively. The velocity field computed using the depth sensitive turbulence model (5) is shown in the Figures 15 and 16, demonstrating that the bottom perturbations increase the bottom friction and reduce the overall velocity intensity and the generated turbulent viscosity, making it rather more uniformly distributed over the liquid horizontal area.

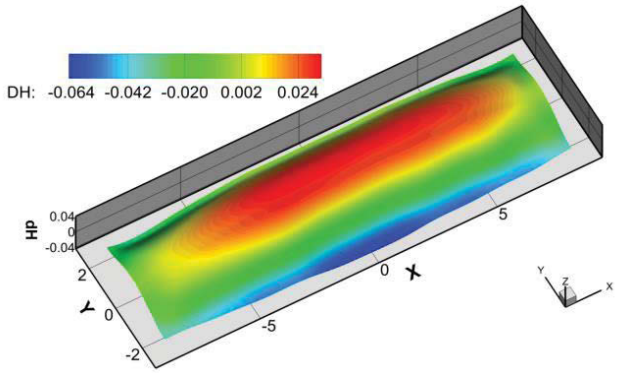

Figure 13. The interface shape for the cell with flat bottom.

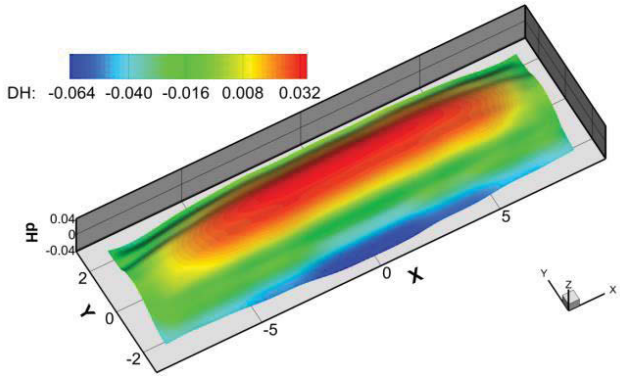

Figure 14. The interface shape for the cell with the cathode perturbations as in the Figure 7.

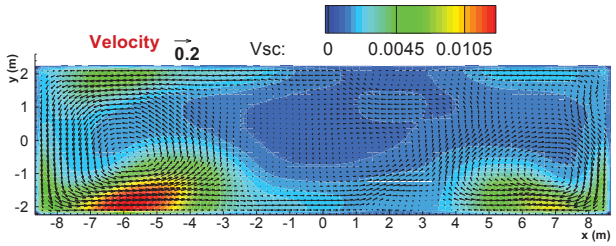

Figure 15. The velocity in liquid aluminium for the cell with flat bottom.

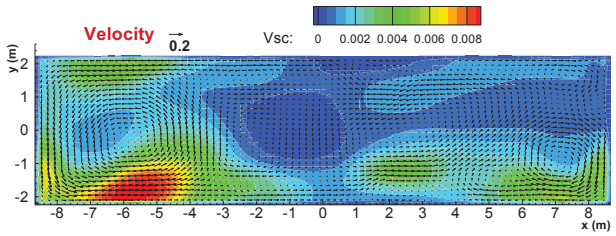

Figure 16. The velocity in liquid aluminium for the cell with the cathode perturbations as in the Figure 7.

3. Anode change perturbation effects

Significant perturbation to the aluminium cell operation is created when one or more anodes are replaced because the old ones have worn out. In this case the electrolyte beneath the new anode freezes and prevents the electric current passage for a significant period of time. The resulting rearrangement of the electric current distribution and the accompanying magnetic field change can create a situation when the MHD stability is seriously disrupted. The practice can be modeled numerically and the best scenarios for the operation involving possible several anode changes in one operation can be found. Figure 17 shows the full cell view of the busbar and anode currents during such an operation when 4 anodes are being replaced.

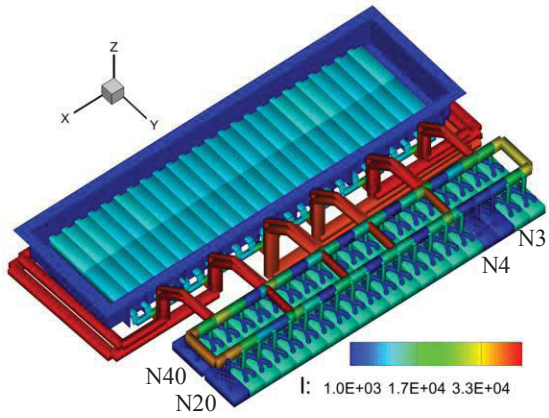

Figure 17. The current distribution in the bus bar network during the anode change of Ns 3, 4, 20, 40.

According to usual convention the anode numbers being replaced are 3, 4, 20, 40 in this case. The corresponding aluminium top surface deformation is shown in the Figure 18, which needs to be compared to the normal interface as shown in the Figure 13. When a different combination of the anodes are replaced, i.e., Ns

7, 8, 29, 30, the corresponding interface is shown in the Figure 19. The dynamic response obtained by the full MHD problem solution as demonstrated in the Figure 20 clearly indicates which operation types are safe to perform and what modification is possibly needed.

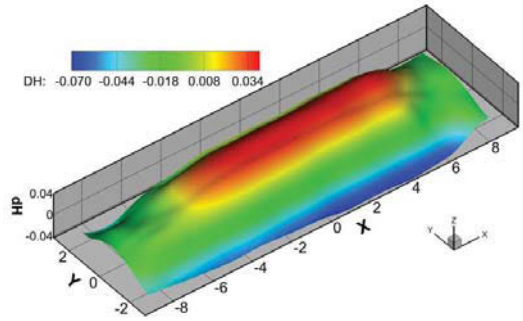

Figure 18. The aluminium top surface shape during the anode change of Ns 3, 4, 20, 40.

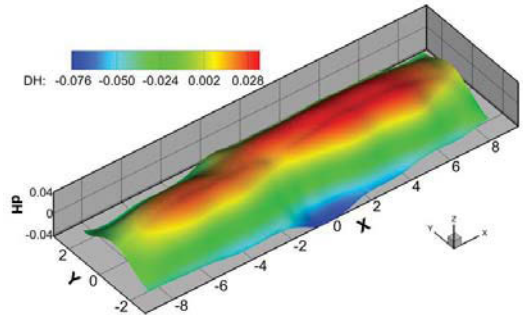

Figure 19. The aluminium top surface shape during the anode change of Ns 7, 8, 29, 30.

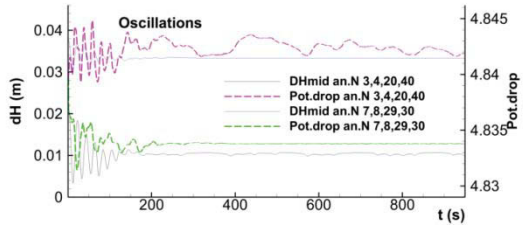

Figure 20. The interface dynamics reflecting the MHD stability change during the two anode change operations.

4. Collector bar disconnection effects

Another type of electric current perturbation can occur if a particular cathode collector is damaged, the flex connection is disrupted and the situation is shown in the Figure 21. This could lead to a serious MHD stability disruption, as shown in the Figure 22. The reason for the disruption is the electric current rearrangement in the liquid metal (Figure 23).

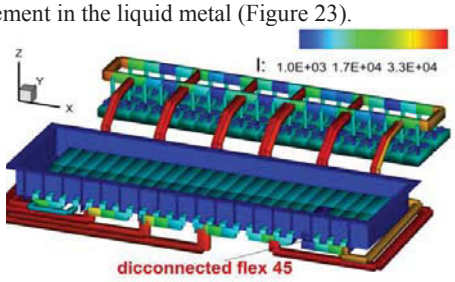

Figure 21. The disconnected collector bar situation.

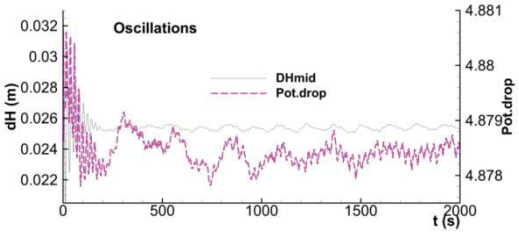

Figure 22. The disconnected collector bar leads to the interface and cell voltage fluctuation.

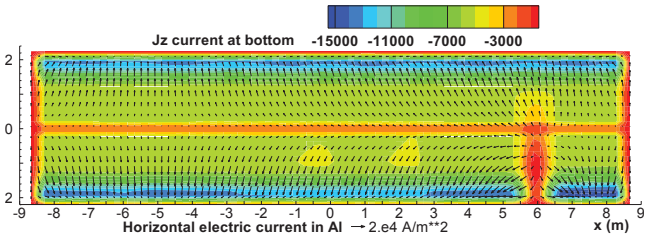

Figure 23. The disconnected collector bar leads to the electric current redistribution in the metal layer.

5. End cells and shunted mid cells

The end of the pot line cells are subject to significant magnetic field difference if compared to the mid line cells. The electric current path requires the full current to transfer from the end of line to the return line or to the power supply. Figure 24 demonstrates the MHD wave disruption for the end of line cell as simulated without any particular bus arrangement to compensate the end cell magnetic field. After a series of numerical experiments the arrangement shown in the Figure 25 was found to give the magnetic field (Figure 26) very closely resembling that of the mid of line cells and preserving the MHD stability (Figure 27).

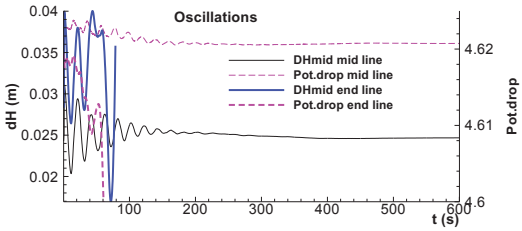

Figure 24. Comparison of the wave behavior for the stable mid pot line cell and the end of line cell without compensation.

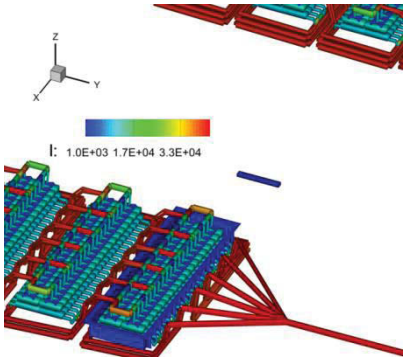

Figure 25. The end of line cell with the optimized compensating bus arrangement.

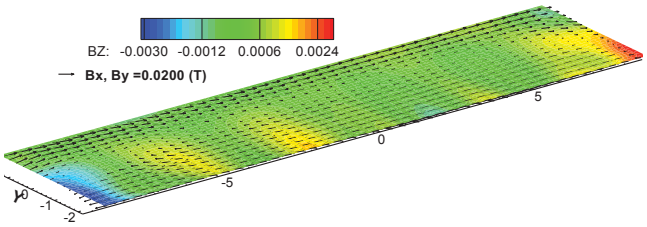

Figure 26. Magnetic field at the liquid metal level for the end of line cell with the optimized compensating bus arrangement.

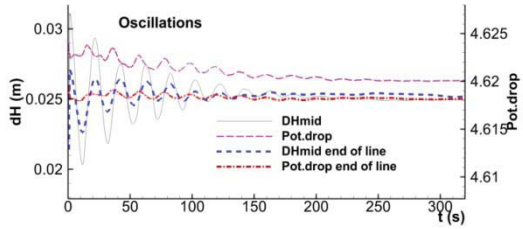

Figure 27. Comparison of the wave behavior for the stable mid pot line cell and the well compensated end of line cell.

In the case of disconnected cell in the mid line position there is a similar procedure available for the purpose to find a suitable current path with the compensating and shunt bars, for instance as shown in the Figure 28. The MHD stability is sussessfully preserved as demonstrated by the modelling results in the Figure 29. Without the optimised shunting bar positioning the cell stability is destroyed, potentially leading to the process disruption for the othe cells in the line.

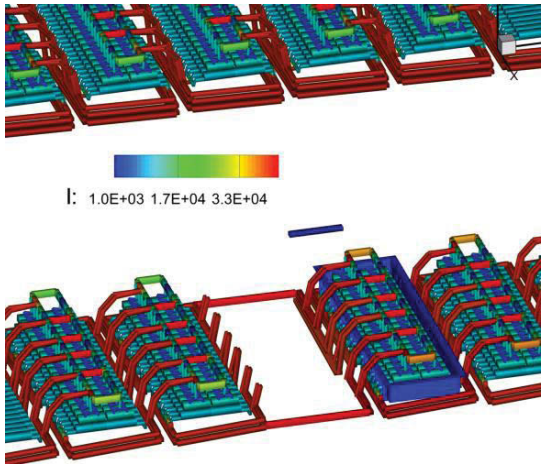

Figure 28. The shunted upstream cell optimised arrangement.

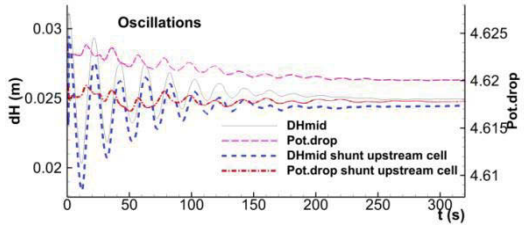

Figure 29. Comparison of the wave behavior for the stable mid pot line cell and the compensated shunted cell case.

Conclusions

The MHD model for the non-linear cell stability analysis software was updated to account for various technological deviations from a normal cell operation practice. The effect of bottom friction enhancing elements is evaluated using various electric current models indicating the importance of the volume conservation and the role of the cathode rod contact resistance. The depth sensitive turbulent velocity model is shown to adjust to the bottom irregularity, leading to the MHD stabilization if the total liquid volume is preserved. The end cells, shunted cells, anode change operation are investigated using the model to predict possible MHD instability and to find optimum practical solutions.

References

1. Urata, N., Mori, K. and Ikeuchi, H. “Behavior of bath and molten metal in aluminium electrolytic cell”. Keikinzoku, 26 (1976), no. 11, pp. 573-600.
2. V. Bojarevics and K. Pericleous, “Solutions for the Metal-Bath Interface in Aluminium Electrolysis Cells”. In Proceedings of TMS Light Metals (2009), pp. 569-574.
3. A. Zarouni, L. Mishra, M. Bastaki, A.A. Jasmi, A. Arkhipov, V. Potocnik, “Mathematical Model Validation of Aluminium Electrolysis Cells at Dubal”, TMS Light Metals, 2013, 597-602.
4. S. Ruan et al., “Production Application Study on Magneto-Hydro-Dynamic Stability of a Large Prebaked Anode Aluminim Reduction Cell”, TMS Light Metals, 2013, 603-607.
5. D.S. Severo, V. Gusberti, A.F. Schneider, E.C. Pinto and V. Potocnik, “Comparison of Various Methods for Modeling the Metal-Bath Interface”. In Proceedings of TMS Light Metals (2008), pp. 413-418.
6. Z. X. Feng. “The treatment of singularities in calculation of magnetic field by using integral method”. *IEEE Magnetics, 1985,* MAG 21, N 6, 2207-2210.
7. D. C. Wilcox. *Turbulence Modelling for CFD*, 2nd ed. (DCW Industries, California, 1998).
8. A.K. Rastogi and W. Rodi. Prediction of heat and mass transfer in open channels. *J. Hydraulics Division ASCE,* HY3 (1978), 397-420.
9. B. Li, F. Wang, X. Zhang, F. Qi, N. Feng. “Development and Application of an Energy Saving Technology for Aluminium Reduction cells”. In Proceedings of TMS Light Metals (2012), pp. 865-868.
10. J. Zhou et al., “Depth Analysis and Potential Exploitation of Energy-Saving and Consumption-Reduction of Aluminum Reduction Pot”, TMS Light Metals, 2012, 601-606.
11. N. Feng et al., “Research and Application of Energy Saving Technology for Aluminum Reduction in China”, TMS Light Metals, 2012, 563-568.
12. V. Bojarevics, “MHD of Aluminium Cells with the Effect of Channels and Cathode Perturbation Elements”, TMS Light Metals, 2013, 609-614.
13. K. Tschope, E. Skybakmoen, A. Solheim. “Cathode wear in Hall-Herault cells”. Aluminium (2013), 1-2, pp. 95-98.